POSITRONICS OF NANOOBJECTS IN POROUS AND DEFECTIVE SILICON- AND QUARTZ-BASED SYSTEMS

V.I. GRAFUTIN, O.V. ILYUKHINA, G.G. MYASISHCHEVA, E.P. PROKOPIEV[1], S.P. TIMOSHENKOV[1], YU.V. FUNTIKOV[1]

UDC 539.124.6

Federal State Unitary Enterprise "State Scientific Center of the Russian Federation – A.I. Alikhanov Institute for Theoretical and Experimental Physics"
(25, Bolshaya Cheremushkinskaya Str., Moscow 117259, Russia),

[1]**Moscow State Institute of Electronic Technology**
(5, Passage 4806, Moscow 124498, Russia; e-mail: epprokopiev@mail.ru)

Positron annihilation spectroscopy (PAS) has been demonstrated to be one of the efficient modern methods for the determination of nanodefect – such as vacancy and vacancy cluster – sizes, the free volume of pores, cavities, and voids, as well as their concentration and chemical composition at annihilation sites in porous systems, some defective materials, and, generally speaking, plenty of technologically important materials and nanomaterials. The results of experimental researches dealing with nanodefects in porous silicon, silicon, single-crystalline quartz, and quartz powders irradiated with protons have been reviewed in brief.

1. Introduction

Positron annihilation spectroscopy (PAS) [1–7] allows the electron structure of perfect crystals to be determined. Moreover, various imperfections, such as vacancies, vacancy clusters, and voids, with especially small dimensions – down to a cubic nanometer – can be revealed with its help in solids and porous systems. PAS mainly includes three methods: the studies of the time distribution of annihilation photons (TDAP), the angular distribution of annihilation photons (ADAP), and the Doppler broadening of the annihilation line at an energy of 0.511 MeV (DBAL) [1,2]. The TDAP method gives information on the electron density at the positron annihilation site, whereas the two others (ADAP and DBAL) provide information on the distribution of electron momenta and on the chemical composition of the nanoobject environment around an annihilation site. The PAS methods are classed into two groups. The methods belonging to the first group use slow positrons, which allows near-surface layers at small depths to be investigated. In the methods of the second group, fast positrons are applied which can penetrate into deep regions ($\geq$ 50 μm) of an object under study and thus provide information on the type, concentration, and distribution of defects over the entire volume of the solid. All those methods are used widely enough for researches in modern materials science, in particular, in atomic and electronic one (see, e.g., works [7–32]).

PAS researches in compacted nanocrystalline metals and alloys [2–8], semiconductors [9–16], and porous silicon [17] brought about the following results [1–7]:

1. The lifetimes of positrons in compacted nanocrystalline metals and alloys, as well as in elementary semiconductors of the germanium or silicon type that were subjected to irradiation with various elementary particles and γ-rays differ from those of free positrons in perfect crystals [6].

2. The fraction of positrons captured onto vacancies grows with pressure in the case of metals and alloys and with the exposure dose of irradiation in the case of semiconductors. This means that the pressure increase gives rise to an enlargement of the area of interfaces in the former case and to the concentration growth of point defects with nanometer-sized dimensions in the case of semiconductors [6].

3. In metal- and alloy-based nanomaterials, positrons are mainly captured by mono- and divacancies located at the interface between neighbor grains (at intergrain junctions) and by nanopores. The latter are either a joint of three neighbor crystallites or a free volume of absent crystallites. Such conclusions can be drawn due to the results of measurements of the positron lifetime in compacted metals and alloys [6,32]. In those specimens, the lifetime of positrons, τ_1, is close to that of positrons at lattice vacancies in the metal bulk, τ_{IV}. It is adopted that the shortest lifetime τ_1 that can be experimentally fixed in the TDAP spectra is caused by the annihilation of positrons at vacancies located at grain interfaces (interface vacancies) and characterized by dimensions less than $0.2 - 0.4$ nm. The intermediate lifetime τ_2 characterizes the positron annihilation in

three-dimensional vacancy agglomerates – these are nanopores, the dimensions of which reach 10 interatomic distances (of about $0.6 - 0.8$ nm). A very long lifetime τ_3 corresponds to the positron annihilation in pores – these are voids, the sizes of which are close to those of crystallites (more than 1 nm). This circumstance gives us a possibility to study the interface structure which governs not only the smallness of grain dimensions, but the majority of nanomaterial properties.

4. In irradiated semiconductors and porous systems, positrons are captured by point defects with an average size of less than 1 nm and pores with an average size of more than 1 nm [1–3, 11–16, 25–27]. The vacancies are mainly mono- and divacancies – and, to a less extent, tetra-, penta-, and hexavacancies – as the most widespread among other radiation-induced defects, for instance, in silicon.

5. Free vacancy volumes that capture positrons at low temperatures in metals and alloys are located at grain interfaces, rather than in crystallites [6].

6. The capture of positrons by crystallites in metals and alloys is hardly probable, because a plastic deformation of metals results in a smaller variation of the positron lifetime than that under the processing of metals in the nanocrystalline state by compacting them [6].

For today, it has been established experimentally that positrons can effectively probe free volumes (mainly vacancies and divacancies) with dimensions below 1 nm in metals, alloys, semiconductors, porous systems, and nanocrystalline compacted materials [1–3, 11–16, 25–27]. The other straightforward methods, including high-resolution transmission electron microscopy and the researches of atomic diffusion, are very difficult to use for studying the interfaces. At the same time, the sensitivity of the positron annihilation method with respect to the concentration of positron-sensitive defects is restricted from below by $10^{14} - 10^{15}$ cm^{-3}.

In monography [6], it is asserted that the issues concerning the interface structure and its atomic density, as well as the influence of nanopores and other free volumes on nanomaterial properties, still remain unexplored and unapprehended. Therefore, one of the key aims of works devoted to studying the nanomaterials by the positron method is to find correlations between the nature, dimensions, and concentration of nanoobjects, on the other hand, and the quality of applied modern materials, on the other hand. For this purpose, i.e. to search such correlations, various methods can be used.

Below, we consider the methods for the determination of the size of nanoobjects, their concentration, and the chemical composition of a medium surrounding nanoobjects. These methods used the experimentally measured parameters of TDAP and ADAP spectra for positrons annihilating in porous systems and elementary semiconductors of the germanium or silicon type, as well as other technologically important materials which were subjected to irradiation by various elementary particles and γ-rays. The methods are based on theoretical ideas developed in works [18–24]. We also discuss various examples of their application.

2. Determination of Sizes and Free Volumes of Vacancies, Pores, and Voids in Porous Systems, Nanomaterials, and Other Technologically Important Materials

A simple model, where a cavity is simulated by a spherical well of radius R_0 with an infinite potential barrier, is used, as a rule, to calculate the pore size. A positron and a positronium are in this cavity, and they annihilate in it. In so doing, a para-positronium (p-Ps) mainly annihilates with its own electron, whereas an ortho-positronium (o-Ps) and a positron annihilate with the electrons provided by the environment that surrounds the cavity. To ensure an opportunity for the pick-off annihilation to run, it is postulated that the wave functions of a positron and a positron that is a part of o-Ps overlap with those of environmental electrons in a boundary region ΔR, so that the radius R of the pore free volume is $R = R_0 - \Delta R$.

Simple quantum-mechanical calculations allow one to present the lifetime τ_3 of a positron and an o-Ps in the cavity in terms of the cavity dimension R_0 and ΔR [19]:

$$\tau = \tau_b \left[\frac{\Delta R}{R_0} - \frac{\sin(2\pi \Delta R/R_0)}{2\pi} \right]^{-1}. \qquad (1)$$

In this formula, τ_b has the meaning of either the positron lifetime ($\tau_b \approx 0.22$ ns [33]) or the spin-averaged lifetime of a positronium in the medium bulk (beyond a pore or a vacancy) ($\tau_b \approx 0.5$ ns [18–24]).

The analysis of the o-Ps annihilation in molecular solids and zeolites with known values of pore radii, which was made in work [19] on the basis of Eq. (1), showed that $R_w \equiv \Delta R = R_0 - R = 1.66$ Å. Generally speaking, the magnitude of R_w depends on the substance nature. Therefore, in our case of silicon and quartz, Eq. (1) can be applied only to estimate the radii of pores. Note that TDAP spectroscopy turned out an especially efficient method for the determination of the pore and micropore

dimensions, as well as the pore distribution over radii in porous systems (adsorbents, zeolites, molecular solid substances, and so on) [6, 18–24].

Let us apply the same quantum-mechanical model of Ps to obtain a relation between the experimental value of the full width half-maximum (FWHM) $\theta_{1/2}$ of a narrow ADAP component and the free volume radius R. In the p-Ps case, the sought relation looks like [19]

$$R = \frac{16.60}{\theta_{1/2}} - R_W, \tag{2}$$

where R and R_W are measured in angströms, and $\theta_{1/2}$ in microradians. Using Eqs. (1) and (2), we can estimate the free volume radii in porous systems, defective materials, and nanomaterials by measuring $\theta_{1/2}$ of the narrow component with the help of the ADAP method. Note that, in the regarded silicon and quartz cases, the approximate formula

$$R \approx R_0 = 16.6/\theta_{1/2}\ [\text{Å}] \tag{3}$$

is to be used, because we have not found the R_W-values for those substances in the literature. In formula (3), $\theta_{1/2}$ is the width of the narrow component in ADAP spectra arising due to the motion of the center of p-Ps masses.

The ADAP method is more advantageous in comparison with the TDAP one, because the former provides orientational dependences of R (along the direction of measured momenta), whereas the latter gives only the averaged values of this quantity. However, the measurements of ADAP spectra consume more time. Below, we present the results of the determination of nanoobject dimensions and concentrations in porous silicon, silicon, single-crystalline quartz irradiated with protons, and quartz powders measured by the ADAP method. The results were obtained in the framework of the calculation techniques reported above. The experimental data were obtained earlier [2, 3, 15–17, 25–27, 31] and in a number of new experiments with single-crystalline quartz and quartz powders.

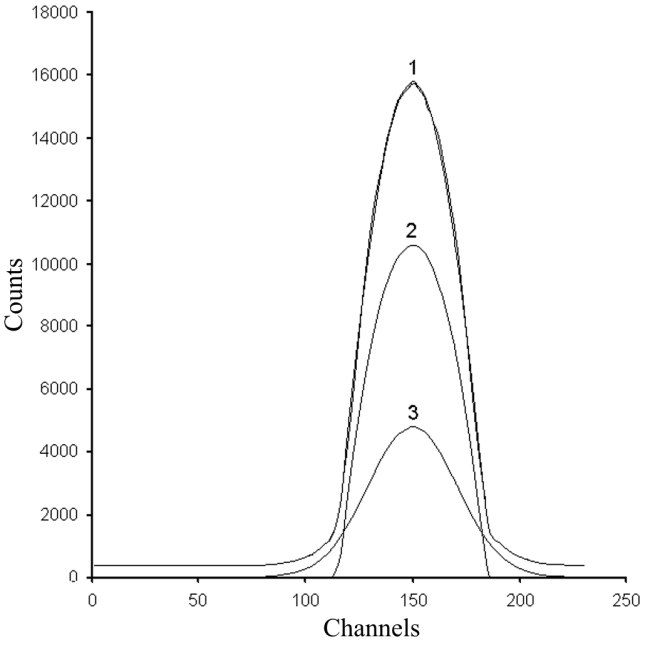

Fig. 1. Angular distributions of annihilation photons in single-crystalline silicon specimens (single-crystalline Si, mirror-polished, p-type, orientation ⟨111⟩, BDS–10, $h = 340$ μm): (*1*) experimental ADAP curve, (*2*) parabolic and (*3*) Gaussian spectral components. Analyzer channels are reckoned along the abscissa axis (1 channel = 0.2 mrad) and the number of events along the ordinate axis

3. Determination of Pore Radius and Concentration in Porous Silicon

The data in Table 1, as well as a comparison between Figs. 1 and 2 in works [17, 25], testify to the presence of p-Ps in porous silicon – see, for instance, porous silicon specimen PR86 (Table 1) and Fig. 2. The experimental ADAP spectra of this specimen are well approximated by a parabola (I_p) and two Gaussians (I_{g1} and I_{g2}). In defect-free silicon crystals (Fig. 1) and in a number of porous silicon specimens [25], these spectra are a superposition of a parabola and a Gaussian. The

T a b l e 1. Parameters of porous silicon specimens, features of their fabrication, and ADAP spectrum characteristics

No. of specimen	Specimen characteristics	$I_{g2} = S_{g1}/S_{\text{sum}}$	$I_{g1} = S_{g1}/S_{\text{sum}}$	$I_p = S_p/S_{\text{sum}}$	Remarks
PR86	porous Si, ⟨111⟩, BDS–0.03, h =360–370 μm, HF:C_2H_5OH=2:1, J =20 mA/cm^2	0.015± 0.003	0.493± 0.052	0.492± 0.044	Porosity ∼45%±3 %

F o o t n o t e: h is the thickness of silicon wafers, ⟨111⟩ is their crystallographic orientation, BDS–0.03 is the mark of boron-doped silicon wafers with a specific resistance of 0.03 Ω × cm, $I_g = S_{gi}/S_{\text{sum}}$ ($i = 1, 2$) are the intensities of Gaussian components, $I_p = S_p/S_{\text{sum}}$ is the parabolic component intensity in ADAP spectra, S_{sum} is the total area of the experimental ADAP spectrum, S_{gi} and S_p are the areas of its Gaussian and parabolic components, respectively, and J is the current density.

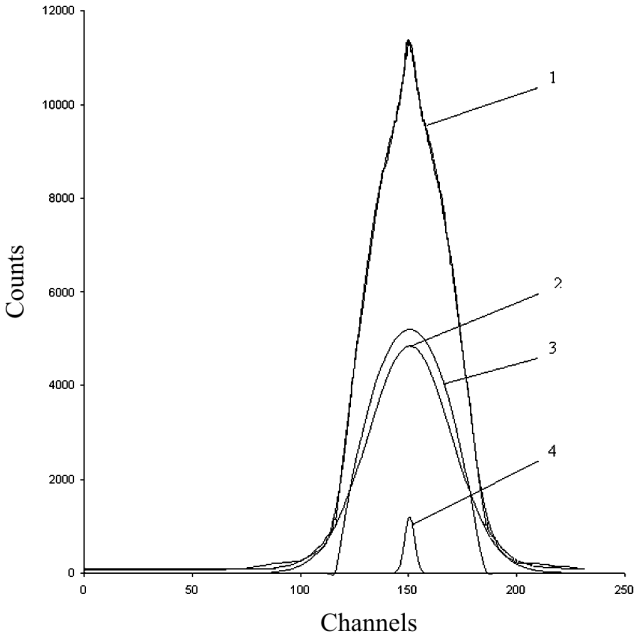

Fig. 2. Angular distributions of annihilation photons in porous silicon specimens (porous Si, ⟨111⟩, BDS–0.03, h = 360 – 370 μm, HF:C_2H_5OH = 2:1, porosity is 45 ± 3%, 2 Gaussians + parabola (see Table 1)): (*1*) total experimental spectrum (the sum of spectra *2*, *3*, and *4*), (*2*) the first Gaussian component, (3) parabolic component, (*4*) the second Gaussian component. Analyzer channels are reckoned along the abscissa axis (1 channel = 0.2 mrad) and the number of coincidences along the ordinate axis

parabolic component can be explained by the annihilation of positrons with electrons from the silicon valence band. At the same time, the wide Gaussian component I_{g1} stems from the multichannel annihilation of positrons and o-Ps in a defect-free part of the crystal in the volume and on the surface of pores, whereas the narrow Gaussian component I_{g2} is a result of the p-Ps annihilation decay in the pore volume. The FWHM of the latter component $(\theta_{1/2})_{g2}$ amounts to about 0.8 mrad, which corresponds to a kinetic energy of the annihilating electron-positron pair of 0.044 eV and its intensity of about 1.5%. In this case, the total yield of positronium in porous silicon reaches about 6%.

To determine the radii of positron traps in porous silicon R_{tr} on the basis of $(\theta_{1/2})_{g2}$-values (see Table 1), we used formula (3). For the experimental value $(\theta_{1/2})_{g2} = 0.8$ mrad (see above), we obtained the average pore radius $R_{\rm tr} \approx 20.75$ Å ≈ 2 nm.

The consideration of the kinetic scheme that describes annihilation decays and transformations of a positron and a positronium in the porous layer enabled us to obtain a relation between the rate $k_{\rm tr}$ of their capture by pores and the component intensity I_{g2} [25]:

$$k_{\rm tr} = t_{g2}\lambda_{\rm cr}\ [{\rm s}^{-1}]. \tag{4}$$

Here, $\lambda_{\rm cr} \approx \lambda_s = 0.8 \times 10^{10}$ s^{-1} is the rate of $p - Ps$ annihilation decay. In its turn, the rate of positron annihilation can be taken equal to $\lambda_{\rm cr} \approx (\lambda_1 = 1/\tau_1)$ [s^{-1}] [31], where τ_1 is the short lifetime of a positron in the crystal, and λ_1 is the corresponding annihilation rate. Substituting the values $I_{g2} \approx 0.015$ (see Table 1) and $\lambda_{\rm cr} \approx 0.8 \times 10^{10}$ s^{-1} into formula (4), we obtain the average rate of p-Ps capture by pores, $k_{\rm tr} = 1.2 \times 10^8$ s^{-1}.

The capture rate $k_{\rm tr}$ can be determined, in turn, on the basis of the well-known expression

$$k_{\rm tr} = \zeta(R_{\rm tr}, T)\sigma_{\rm tr} v N_{\rm tr}\ [{\rm s}^{-1}]. \tag{5}$$

Here, $\zeta(R_{\rm tr}, T)$ is the dimensionless probability of the positron or positronium capture by pores that depends on the pore radius $R_{\rm tr}$ and the temperature T [32], $\sigma_{\rm tr}$ is the average cross-section of the positronium and positron capture by defects, v is the velocity of a thermalized positronium or positron, and $N_{\rm tr}$ is the average concentration of defects (in the defective region of the crystal) that are sensitive to thermalized bulk states of a positronium and a positron. Hence, the given expressions allow the quantities $k_{\rm tr}$, $N_{\rm tr}$, and $R_{\rm tr}$ to be determined, provided that such parameters as λ_1, $\sigma_{\rm tr}$, and v are known. The average thermal velocity of a positronium and a positron at room temperature T = 293 K was evaluated by the formula $v = (8k_0T/\pi m_+^*)^{1/2} \approx 7.52 \times 10^6$ cm/s, where k_0 is the Boltzmann constant, $m_+^* = 2m_0$ is the effective mass of p-Ps, and $m_0 = 9.1 \times 10^{-28}$ g is the free positron mass. We assume that the cross-section of positron and positronium capture by pores is equal to the average geometrical cross-section of a defect $\sigma_{\rm tr} \approx \pi R_{\rm tr}^2$.

Taking $R_{\rm tr} \approx 20 \times 10^{-8}$ cm and $\zeta(R, T) \approx 1$ and using the values of $k_{\rm tr}$ and v calculated above and formula (5), we determined the average concentration of p-Ps capture centers in the porous silicon layer to be $N_{\rm tr} = k_{\rm tr}/(\sigma_{\rm tr} v) = 1.2 \times 10^8/(3.14 \times 4 \times 10^{-16} \times 7.52 \times 10^8) \approx 1.27 \times 10^{14}$ cm^{-3}. According to these data, we may assume that the effective free centers (the regions of positronium capture) are most likely ultramicropores and micropores with dimensions ≤ 2 nm in the porous silicon layer. These estimations are in satisfactory agreement with estimations of the pore size done by formula (1), which we obtained earlier in

work [2] for porous silicon using the data of the TDAP method.

Knowing the total porosity (45%) and the average pore volume, we can evaluate the concentration of pores on the basis of simple geometrical considerations. By comparing it with the calculated N_{tr}, we verify the reliability of the accepted approximations. The average size of a pore determined by us, $R_{\rm tr} \approx 2$ nm, corresponds to its average volume $V_{\rm tr} = \frac{4}{3}\pi R_{\rm tr}^3 = 3.35 \times 10^{-20}{\rm cm}^3$. In the case of "close packing" of such pores and the total porosity equal to 0.45, the pore concentration could be equal to $N_{\rm tr}^G \approx 0.45/V_{\rm tr} \approx 1.35 \times 10^{19}$ cm^{-3}. The discrepancy between this value and the concentration $N_{\rm tr} = 1.3 \times 10^{14}$ cm^{-3} determined by us is too large, which probably testifies to a contribution of very large volumes of pores and voids with larger dimensions to the volume of the porous silicon layer. Any comments on this matter would be premature in this paper. The role of nanoobjects in porous silicon should also be comprehended.

Hence, the results obtained allow us to hope for that the further research will make it possible to connect the parameters of annihilation spectra with pore dimensions and pore topology.

4. Determination of Pore Radius and Concentration in Silicon Wafers Irradiated with Protons

The $10 \times 20 \times 10$-mm^3 specimens under study were cut out from unbroken wafers of n-silicon with the $\langle 100\rangle$ orientation. Four specimens designated below as Si10 (the initial, nonirradiated specimen), Si12, Si14, and Si15 (these are silicon specimens irradiated by protons with the energy E and the fluence Φ) were chosen for researches. The parameters of investigated silicon wafers, the features of their fabrication, and the key characteristics of their ADAP spectra are listed in Table 2.

According to the results of works [15, 16, 26], the difference between the intensities of Gaussian components of the irradiated silicon wafer, I_g(irr), and the initial – nonirradiated – one, I_g(nonirr), in the corresponding ADAP spectra can be written down in the form

$$\Delta I_g = I_g({\rm irr}) - I_g({\rm nonirr}) \sim k_{\rm tr}\tau_1, \tag{6}$$

i.e. the average capture rate amounts to

$$k_{\rm tr} \sim \Delta I_g/\tau_1, \tag{7}$$

where

$$k_{\rm tr} = \frac{1}{i}\sum_i g_i (k_{\rm bi})_{\rm tr}. \tag{8}$$

In formulas (6) and (7), τ_1 is the short lifetime of a positron in the silicon crystal, g_i is the statistical weight of the "defect state" of the i-th positron contributing to the common annihilation process, and $k_{\rm bi}$ is the rate of capture into the i-th state. The quantity k_{bi} can be determined, in turn, by a formula like expression (4). According to Eq. (4), for $\Delta I_g = 0.293 - 0.256 = 0.037$ [26] (see the I_g-values in the last and the first row of Table 2, respectively) and $\tau_1 = 2.19 \times 10^{-10}$ s, we obtain $k_{\rm tr} \approx 1.7 \times 10^8$ s^{-1}.

We can also find the dimensions of vacancies, vacancy complexes, and pores, as well as the energies E, making use of only ADAP data, if we suppose the

T a b l e 2. Parameters of porous silicon specimens, features of their fabrication, and ADAP spectrum characteristics

No. of specimen	Substance	$(\theta_g)_{1/2}$, mrad	$Ig = Sg/S_{\rm sum}$	$(\theta_p)_{1/2}$, mrad	$I_P = S_p/S_{\rm sum}$	Remarks
Si 10	Si, $\langle 100\rangle$, PDS–4.5, h=455 μm, n-type	11.0 ± 0.3	0.256± 0.04	6.98	0.744± 0.049	
Si 12	Si, $\langle 100\rangle$, PDS–4.5 h =415 μm	11.1 ± 0.32	0.256 ± 0.04	6.93	0.735± 0.051	proton-irradiated E=40 keV, Φ=5×10^{16} cm^{-2}
Si 14	Si, $\langle 100\rangle$, PDS 2–3, h =418 μm	11.1 ± 0.27	0.283 ± 0.04	6.94	0.717 ± 0.045	proton-irradiated E=150 keV, Φ = 4×10^{16} cm^{-2}
Si 15	Si, $\langle 100\rangle$, PDS 2–3 h =418 μm	11.1 ± 0.28	0.293 ± 0.041	6.81	0.707 ± 0.047	proton-irradiated E=150 keV, Φ = 4×10^{16} cm^{-2}

F o o t n o t e: h is the thickness of silicon wafers, $\langle 100\rangle$ is their crystallographic orientation, PDS–4.5 is the mark of phosphor-doped silicon wafers with specific resistances of 4.5 and $2-3\ \Omega \times$ cm, E is the energy of protons, Φ is their fluence, $(\theta_g)_{1/2}$ is the width of the Gaussian component with intensity $I_g = S_g/S_{\rm sum}$, θ_p is the cutoff angle for the parabolic component with intensity $I_p = S_p/S_{\rm sum}$ in ADAP spectra ($S_{\rm sum}$ is the total number of coincidences, S_g and S_p are the rates of coincidence count for the Gaussian and parabolic components, respectively, in ADAP curves).

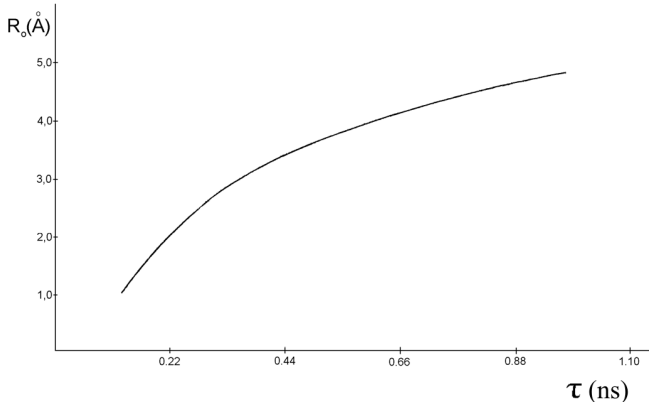

Fig. 3. Dependence of the positron lifetime τ in pores on the effective pore radius R_0 (Eq. (1)) for $\Delta R = 1.66$Å [19] and $\tau_b = 0.219$ ns [33]

spherical geometry of those objects at a site of the positron annihilation with external valence electrons. Really, the dispersion σ of Gaussian components in ADAP spectra approximated by the normal law of error distribution is unambiguously connected with the energy E of an annihilating electron-positron pair located in a pore with radius $R_{\rm tr}$:

$$E = \frac{3}{2}\frac{mc^2}{2}\sigma^2, \tag{9}$$

where $\sigma = \frac{(\theta_{1/2})_g}{2\sqrt{2\ln 2}} = 0.425(\theta_{1/2})_g$. Here, $(\theta_{1/2})_g$ is the FWHM of the ADAP curve. Since the majority of works give the FWHM rather than the dispersion σ, let us write down an expression for the dependence of the energy of annihilating electron-positron pairs on the FWHM:

$$E = 6.9 \times 10^{-2}(\theta_{1/2})_g^2. \tag{10}$$

Here, the energy E is reckoned in electronvolts and the FWHM $(\theta_{1/2})_g$ in microradians.

In particular, the measured value of $(\theta_{1/2})_g$ is 11.1 mrad for silicon specimens (see Table 2), which corresponds to the average energy of annihilating electron-positron pairs $E = 8.5$ eV. Such a value is due to the average energy of electrons in the external shell of a silicon atom at the pore wall, which can be adopted equal to the energy of an electron in the external shell of an isolated silicon atom. In so doing, we take into account that the positron and the positronium have enough time to get thermalized before annihilation, and that the measured energy is mainly determined by the energy of an electron. The tabulated value of the energy for the external electron shell of a silicon atom, Si($3p^2 - {}^3P_0$), is E(Si) = 8.1517 eV [28]. As we see, the agreement between those energy values is quite satisfactory. Therefore, positrons mainly annihilate with external valence electrons of silicon atoms belonging to the pore "wall". We may assume that the difference $E - E(\mathrm{Si}) = 0.35$ eV follows from the contribution to the energy of the annihilating electron-positron pair given by a positron located in the spherical defect.

We also used Eq. (1) to determine the radii of vacancy free volumes from the experimental (the TDAP method) values of positron lifetimes in silicon irradiated with electrons and protons [33–37]. We suggested that, in our case, the moderate proton energies and proton exposure doses would be enough, and that point defects were predominately generated in the course of silicon wafer irradiation [33]. The positron lifetime falls within the interval from 266 to 270 ps in monovacancies and from 300 to 325 ps in divacancies. In tetravacancies, this quantity is equal to 435 ps, in pentavacancies to 505 ps, and in hexavacancies to about 520 ps [33–37]. In Fig. 3, the dependence of those τ-values on R_0 (formula (1)) is plotted. The average effective radius of radiation-induced defects, which can be determined by formula (1), amounts to $R_{\rm tr} \equiv R_0 \approx 1.7$ Å for the average lifetime.

Therefore, if we consider that a vacancy or a pore (a potential well) contains a positron rather than a positronium and that the positron annihilates with electrons of the wall material, its energy in the well should be of the order of 0.35 eV at $E = 11.1$ eV. Since the energy of a particle in a potential well is determined by the well dimensions, such a positron energy – according to formula (2) – should correspond to the well radius $\bar{R}_{\rm tr} \leq 10.4$ Å for $(\theta_{1/2})_g = 11.1$ mrad. A rather large discrepancy between the $R_{\rm tr}$-values determined in the framework of the TDAP and ADAP methods can be explained either by methodological errors or by the fact that the TDAP method allows the averaged values $\bar{R}_{\rm tr}$ to be determined in the spherical approximation for vacancy defects, whereas the ADAP method can provide the orientational dependences of $R_{\rm tr}$ (along the direction of measured momenta). According to the microscopic theory of vacancy defects (for instance, for a vacancy in silicon [38]), the orientational dependences of electron properties of a vacancy along various crystallographic directions demonstrate appreciable features. It happens that a vacancy has four charging states – V^+, V^0, V^-, and V^{--} – but only the last two of them can be observed using the EPR method. Probably, the ADAP method gives a possibility to observe the dependences of the electron properties of the vacancy walls and their dimensions on the crystallographic direction. The further careful researches in this direction are needed.

The lattice constant of silicon is equal to $a = 5.43$ Å, and the corresponding average interatomic distance is $r_{\rm Si} = 2.087$ Å. The radius values measured following the TDAP method are $R_{\rm tr} \approx 1.7$ Å and $r_{\rm Si} = 2.087$ Å, which evidences for a satisfactory character of the models used. Again, the value $R_{\rm tr} \approx 1.7$ Å gives rise to the average cross-section of positron capture by defects $\sigma_{\rm tr} \approx \pi R_{\rm tr}^2 \approx 9 \times 10^{-16}$ cm^2. In order to estimate the average concentrations of radiation-induced defects making use of formula (4), we take that $k_{\rm tr} \approx 1.7 \times 10^8$ s^{-1}, $\sigma_{\rm tr} \approx 8 \times 10^{-16}$ cm^2, and $v \approx 10^7$ cm/s. For the concentration of radiation-induced defects, we obtain $N_{\rm tr} \approx 2 \times 10^{16}$ cm^{-3} in the case of n-silicon with orientation (100) [26] and $N_{\rm tr} = 10^{16} \div 10^{17}$ cm^{-3} in the case of p-silicon with orientation (111) [15,16] (see Tables 2 to 5). All the abovesaid allows us to suggest that radiation-induced defects of the monovacancy V type and their complexes [29, 30] predominantly manifest themselves in the studied n- and p-silicon wafers subjected to proton irradiation. It is point-like radiation defects with dimensions (diameters) ranging from 2 to 10 Å that are the effective centers of positron capture [26]. Hence, the positron method allows the concentrations of point-like radiation-induced defects with dimensions ≤ 1 nm in silicon to be effectively estimated. Such defects are practically inaccessible for observation in the framework of other available methods. Note that it is the positron methods that allowed the fact that point defects play a

T a b l e 3. Parameters of *p*-Si specimens and features of their fabrication

No. of specimen	Specimen characteristics	Remarks
164(1)	single-crystalline Si, mirror-polished, ⟨111⟩, BDS–10, $h = 340$ μm	class 11 surface finish
165(2)	single-crystalline Si, mirror-polished, ⟨111⟩, BDS–10, $h = 340$ μm, proton-irradiated ($E = 3$ MeV, $\Phi = 1.03 \times 10^{16}$ cm^{-2})	class 11 surface finish
163(3)	single-crystalline Si, mirror-polished, ⟨111⟩, BDS–10, $h = 340$ μm, proton-irradiated ($E = 3$ MeV, $\Phi = 4.3 \times 10^{16}$ cm^{-2})	class 11 surface finish
153(4)	single-crystalline Si, polished, ⟨111⟩, BDS–10/20, $h = 490$ μm, $\rho = 9.8$–10.0 Ω × cm	
166(5)	single-crystalline Si, polished, ⟨111⟩, BDS–10/20, $h = 490$ μm, $\rho = 9.84$–10.0 Ω × cm, proton-irradiated ($E = 3$ MeV, $\Phi = 5.15 \times 10^{15}$ cm^{-2})	
152(6)	single-crystalline Si, ground, p-type, ⟨111⟩, BDS–10, $h = 500$ μm, $\rho = 8.6$ Ω × cm	
154(7)	single-crystalline Si, ground, p-type, ⟨111⟩, BDS–10, $h = 500$ μm, $\rho = 8.6$ Ω × cm, proton-irradiated ($E = 3$ MeV, $\Phi = 6.88 \times 10^{15}$ cm^{-2})	22-mm beam shift with respect to target center
155(8)	single-crystalline Si, ground, p-type, ⟨111⟩, BDS–10, $h = 500$ μm, $\rho = 8.6$ Ω × cm, proton-irradiated ($E = 3$ MeV, $\Phi = 7 \times 10^{15}$ cm^{-2})	Beam centered on the target
162(9)	single-crystalline Si, ground, p-type, ⟨111⟩, BDS–10, $h = 500$ μm, $\rho = 8.6$ Ω × cm, proton-irradiated ($E = 3$ MeV, $\Phi = 1.9 \times 10^{16}$ cm^{-2})	

T a b l e 4. ADAP spectrum characteristics of *p*-Si specimens and parameters of radiation-induced defects

No. of specimen	$I_g = S_g/S_{\rm sum}$	$I_p = S_p/S_{\rm sum}$	$k_{\rm tr} \times 10^{-9}$, s^{-1}	$R_{\rm tr}$, Å	$N_{\rm tr} \times 10^{-17}$, cm^{-3}
164(1)	0.335±0.031	0.665±0.035			
165(2)	0.600±0.030	0.400±0.022	1.2	1.6	1.5
163(3)	0.589±0.028	0.411±0.021	1.15	1.6	1.4
153(4)	0.330±0.029	0.670±0.034		1.6	
166(5)	0.373±0.032	0.627±0.034	0.19	1.6	0.2
152(6)	0.305±0.029	0.695±0.035			
154(7)	0.446±0.049	0.554±0.047	0.63	1.6	0.6
155(8)	0.332±0.029	0.668±0.035	–	–	–
162(9)	0.512±0.026	0.488±0.022	0.93	1.6	1.0

dominant role in various defective solids to be established directly.

5. Determination of Free Volume Radius and Concentration in Quartz Single Crystals Irradiated with Protons

Our experiments [31] showed that, when completely thermalized atoms of p-Ps annihilate in quartz single crystals in the temperature interval 288–633 K, the FWHM of the narrow component with intensity I_{g2} is $(\theta_{1/2})_{g2} \approx 1.03 \div 1.25$ mrad only. For the wide component with intensity I_{g1}, its FWHM $(\theta_{1/2})_{g1} \approx$ 10 mrad (see Table 6). These data allow us to speak about the presence of p-Ps in quartz single crystals. The total yield of positroniums in quartz reaches a value of about 12%, and their energy ranges from 0.025 to 0.06 eV. It should be noted that the interaction between a delocalized p-Ps and the quartz crystal lattice invokes the appearance of lateral peaks in the spectrum at angles that are inversely proportional to the reciprocal lattice vector. At the same time, these lateral peaks are completely absent from the spectra of those single-crystalline quartz specimens that contain as high concentrations of impurities as possible [31]. This circumstance may probably testify that a p-Ps atom is localized in this case in quartz single crystals which contain the highest concentrations of impurities or radiation-induced defects in a region (a cavity) with a certain volume and the radius equal—by the order of magnitude—to the quartz lattice constant. The average value of the radius of this cavity, in which the annihilation of positronium in quartz occurs and which is simulated by a potential well with radius $R_{\rm tr}$ and an infinite potential barrier, evaluated by formula (3) is also quoted in Table 5. Note that the dependence of the narrow component intensity $I_{g2} = S_2/S_{\rm sum}$ (Table 6) on the temperature is rather weak, which, in general, satisfies the theoretical dependence of I_{g2} obtained in works [24,25]. Here, S_2 is the coincidence count rate, i.e. the area that corresponds to the intensity I_{g2} in ADAP spectra, and $S_{\rm sum}$ is the total number of coincidences. The data in Table 6 demonstrate that the p-Ps atom localization radius varies with temperature from 16.3 Å at 288 K to 13.3 Å at 623 K. Such an abnormal dependence of $R_{\rm tr}$ can hardly be explained in the framework of the calculation model in use. However, it can be explained in the framework of the concept of p-Ps quasiparticle state which arises owing to the interaction between this localized atom and vibrational states of crystal structural defects (Ps–phonon interaction) [39, 40]. In this case, the effective mass of p-Ps decreases with the temperature growth. This is nothing more than a quantum-mechanical effect caused by the damping of the positronium quasiparticle state in the crystal. Such an effect is accompanied by a growth of $(\theta_{1/2})_{g1}$-values and, therefore, by a reduction of $R_{\rm tr}$ (Table 6). Making use of the data quoted in Table 6, we determined the concentration of the p-Ps capture centers in quartz: at $R_{\rm tr} \approx 12 \times 10^{-8}$ cm and $I_{g2} \approx 0.03$, $N_{\rm tr} = k_{\rm tr}/(\sigma_{\rm tr} v) = I_{g2}\lambda_{\rm tr}/(\pi R_{\rm tr}^2 v) \approx 4.2 \times 10^{-14}$ cm^{-3}. According to these data, we can suggest that the effective free centers (the regions of positronium capture) are most likely vacancies or divacancies that emerge due to the elastic stresses induced by interstitial impurities and radiation defects in the bulk of a quartz crystal [31].

6. Determination of Pore Free Volume Radius and Pore Concentration in Quartz Powders

When quartz powders contained particles with various dimensions, the ADAP spectra could be decomposed

T a b l e 5. Parameters of *p*-Si specimens, features of their fabrication, and ADAP spectrum characteristics

No. of specimen	Specimen characteristics	$I_g = S_g/S_{\rm sum}$	$I_p = S_p/S_{\rm sum}$	$N_{\rm tr} \times 10^{-16}$, cm^{-3}
164(1)	single-crystalline Si, mirror-polished, $\langle 111\rangle$, BDS–10, $h = 340$ μm			
153(4)	single-crystalline Si, polished, *p*-type, $\langle 111\rangle$, BDS–10/20, $h = 490$ μm, $\rho = 9.8 - 10.0$ $\Omega \times$ cm	0.330±0.029	0.670±0.034	1.63
152(6)	single-crystalline Si, ground, *p*-type, $\langle 111\rangle$, BDS–10, $h = 500$ μm, $\rho = 8.6$ $\Omega \times$ cm	0.305±0.029	0.695±0.035	1.60

F o o t n o t e: h is the thickness of silicon wafers, $\langle 111\rangle$ is their crystallographic orientation, BDS–10 and BDS–10/20 are the mark of boron-doped silicon wafers, E and Φ are the energy and the fluence of protons, respectively, $I_g = S_g/S_{\rm sum}$ *is* the intensity of Gaussian component, $I_p = S_p/S_{\rm sum}$ is the intensity of parabolic component in ADAP spectra, $S_{\rm sum}$ is the total area of the experimental ADAP spectrum, S_g and S_p are the areas of its Gaussian and parabolic components, respectively.

T a b l e 6. Parameters of positron annihilation in quartz at various temperatures

T, K	$(\theta_{1/2})_{g2}$, mrad	I_{g2}	$(\theta_{1/2})_{g1}$, mrad	I_{g1}	$R_{\rm tr}$, Å
633	1.25÷0.05	0.0300÷0.0026	10.70÷0.05	0.9700÷0.0210	13.3
473	1.18÷0.04	0.0326÷0.0021	11.00÷0.04	0.9674÷0.0170	14.1
288	1.02÷0.05	0.0359÷0.0041	10.70÷0.09	0.9641÷0.0320	16.3

T a b l e 7. Results of the processing of the experimental data for quartz powder specimens by an ACARFIT computer code

No. of specimen	Number of components	FWHM $(\theta_{1/2})_{gi}$, mrad			I_{gi} %			$R_{{\rm tr}i}$, Å	
		$(\theta_{1/2})_{g1}$	$(\theta_{1/2})_{g2}$	$(\theta_{1/2})_{g3}$	I_{g1}	I_{g2}	I_{g3}	$R_{\rm tr2}$	$R_{\rm tr3}$
N1	2G	9.5	1.7	–	90	10	–	9.76	
	3G	9.6	2.5	1.3	88	8	4	6.6	12.8
N2	2G	9.1	1.7	–	83	17	–	9.8	
	3G	9.5	2.6	1.1	79	13	8	6.4	15
N3	2G	8.6	1.8	–	86	14		9.2	
	3G	9.1	2.4	1.0	84	12	4	6.9	16.6
N4	2G	9.3	1.4	–	76	24	–	11.9	
	3G	9.5	1.6	0.6	76	22	2	10.4	28
N5	2G	9.5	1.4	–	82	18	–	11.9	
	3G	9.7	2.0	1.2	81	10	9	8.3	13.8

into two ($\chi^2 \sim 1.7$) or three ($\chi^2 \sim 0.6$) components with intensities I_{gi} and widths $(\theta_{1/2})_{gi}$ (Table 7). Basing on the χ^2-values, we preferred the case with three components. The results of the mathematical processing of ADAP spectra with the help of an ACARFIT computer code (see Table 1) demonstrate that the spectra of all quartz powder specimens include a high-intensity ($I_{g2} = 10 - 24\%$), narrow positronium component ($(\theta_{1/2})_{g2} \approx 1$ mrad). The parameter σ of the wide Gaussian component remained practically constant (of about 4 mrad). Since the narrow component intensity does not exceed 5% in single-crystalline quartz [31], the emergence of the high-intensity positronium component is associated with the presence of nano-sized pores and the surface of powder microparticles [42].

We connect the component characterized by the intensity I_{g1} and the width $(\theta_{1/2})_{g1}$ with the annihilation of positrons and o-Ps positrons, on the one hand, and the valence electrons of quartz, on the other hand (most likely, the electrons of oxygen anions in quartz (free collisions) and the electrons belonging to the bound states of the positron–anion quasiatomic systems [41]). The components with intensities I_{g3} and I_{g3} and widths $(\theta_{1/2})_{g2}$ and $(\theta_{1/2})_{g3}$ were associated with the annihilation of p-Ps captured by various traps with radii $R_{\rm tr2}$ and $R_{\rm tr3}$, respectively, distributed over the powder volume. In this case, we used formula (3) to determine the radii $R_{\rm tr2}$ and $R_{\rm tr3}$. For $(\bar{\theta}_{1/2})_{g2} \approx 1.91$ mrad, $\bar{I}_{g2} = 14.8\%$, and $\bar{R}_{\rm tr2} = 9$ Å, we obtained the average concentration of $tr2$-traps $(\bar{N}_{\rm tr})_2 \approx 5.8 \times 10^{15}$ cm^{-3}; and for $(\bar{\theta}_{1/2})_{g3} \approx 1.04$ mrad, $\bar{I}_{g3} = 5.4\%$, and $\bar{R}_{\rm tr3} = 16.0$ Å, we obtained the average concentration of tr3-traps $(\bar{N}_{\rm tr})_3 \approx 5.8 \times 10^{14}$ cm^{-3}. On the basis of these results, we may assume that tr2-traps include p-Ps capture centers in the near-surface region of quartz particles (nano-sized pores and the surface of powder microparticles), whereas tr3-traps include pores in the bulk of quartz microparticles [42].

Thus, our researches of the positron annihilation in quartz powders have showed that positrons can effectively probe various free volumes in these quartz specimens.

7. Conclusion

By applying the ADAP method, we have determined the chemical composition of the quartz medium at the site of the positron annihilation with external valence electrons of silicon atoms at the vacancy (pore) "wall", as well as the dimensions and the concentration of nano-sized defects in a number of defective materials, in particular, in wafers of single-crystalline silicon, quartz single crystals irradiated with protons, and quartz powders.

1. V.I. Goldanskii, At. Energy Rev. **6**, 3 (1968).
2. V.I. Grafutin and E.P. Prokopiev, Usp. Fiz. Nauk **172**, 67 (2002).
3. E.P. Prokopiev, S.P. Timoshenkov, V.I. Grafutin, G.G. Myasishcheva, and Yu.V. Funtikov, *Positronics of Ionic Crystals, Semiconductors, and Metals* (MIET, Moscow, 1999) (in Russian).
4. I.Ya. Dekhtyar, Phys. Rep. **9**, 5 (1974).

5. A.P. Druzhkov and D.A. Perminov, in *Nuclear Materials Research Developments,* edited by J.F. Keister (Nova Science Publishers, New York, 2007), Chap. 5.

6. A.I. Gusev, *Nanomaterials, Nanostructures, Nanotechnologies* (Fizmatlit, Moscow, 2005) (in Russian).

7. R. Wurschum and H.-E. Schaefer, in *Nanomaterials: Synthesis, Properties, and Applications,* edited by A.S. Edelstein and R.C. Cammarata, (Institute of Physics, Bristol, 1996), p. 277.

8. A.A. Rempel, *Ordering Effects in Non-Stoichiometric Interstitial Compounds* (Nauka, Ekaterinburg, 1992) (in Russian).

9. R. Krause-Rehberg and H.S. Leipner, *Positron Annihilation in Solids. Defect Studies* (Springer, Berlin, 1999).

10. V.V. Batavin, A.P. Druzhkov, A.E. Garnak, A.D. Mokrushin, E.P. Prokopiev, and F.R. Khashimov, Microelektronika **9**, N 1, 120 (1980).

11. E.P. Prokopiev, Poverkhnost N 10, 91 (1993).

12. V.A.Fedorov, V.I. Prilipko, E.P. Prokopiev, and K.P. Arefiev, Izv. Vyssh. Ucheb. Zaved. Fiz. N 5, 40 (1982).

13. K.P. Arefiev, V.I. Prilipko, E.P. Prokopiev, and V.A. Fedorov, Izv. Vyssh. Ucheb. Zaved. Fiz. N 8, 117 (1983).

14. V.I. Prilipko and E.P. Prokopiev, Elektron. Promyshl. N 11–12, 20 (1980).

15. O.M. Britkov, S.A. Gavrilov, V.I. Grafutin, V.V. Dyagilev, V.V. Kalugin, O.V. Ilyukhina, G.G. Myasishcheva, E.P. Svetlov-Prokopiev, S.P. Timoshenkov, and Yu.V. Funtikov, Vopr. At. Nauki Tekhn. Ser. Teor. Prikl. **3**, 40 (2004).

16. V.I. Grafutin, O.V. Ilyukhina, V.V. Kalugin, G.G. Myasishcheva, E.P. Prokopiev, Yu.V. Funtikov, An.S. Timoshenkov, D.K. Grigoriev, and S.P. Timoshenkov, Fiz. Khim. Obrab. Mater. N 5, 5 (2006).

17. S.A. Gavrilov, V.I. Grafutin, O.V. Ilyukhina, G.G. Myasishcheva, E.P. Prokopiev, S.P. Timoshenkov, and Yu.V. Funtikov, Pis'ma Zh. Eksp. Teor. Fiz. **81**, 680 (2005).

18. E.P. Prokopiev, in *Abstracts of the 46-th Conference on Nuclear Spectroscopy and Atomic Kernel Structure* (PIYaF, Saint Petersburg, 1996), p. 377 (in Russian).

19. Y.C. Jean, Microchem. J. **42**, 72 (1990).

20. B. Gregory Roger, J. Appl. Phys. **70**, 4665 (1991).

21. S.J. Tao, J. Phys. Chem. **56**, 5499 (1972).

22. M. Eldrup, D. Lightbody, and J.N. Sherwood, Chem. Phys. **63**, 51 (1981).

23. V.P. Shantarovich, Yu.P. Yampol'skii, and I.B. Kevdina, Khim. Vysok. Energ. **28**, 55 (1994).

24. I.B. Kevdina, Yu.M. Sivergin, and V.P. Shantarovich, Khim. Vysok. Energ. **30**, 145 (1996).

25. O.M. Britkov, S.A. Gavrilov, V.I. Grafutin *et al.*, Peterburg. Zh. Elektron. N 3, 15 (2007).

26. V.I. Grafutin, O.V. Ilyukhina, G.G. Myasishcheva, V.V. Kalugin, E.P. Prokopiev, S.P. Timoshenkov, N.O. Khmelevskii, and Yu.V. Funtikov, Mikroelektronika **34**, 218 (2005).

27. V.I. Grafutin, A.G. Zaluzhnyi, S.P. Timoshenkov, O.M. Britkov, O.V. Ilyukhina, V.P. Komlev, G.G. Myasishcheva, E.P. Prokopiev, and Yu.V. Funtikov, Poverkhnost 2008 (to be published).

28. A.P. Babichev, N.A. Babushkina, A.M. Bratkovskii *et al.*, *Physical Constants: A Reference Book,* edited by I.S. Grigoriev and E.Z. Melikhov (Energoatomizdat, Moscow, 1991) (in Russian).

29. V.A. Kozlov and V.V. Kozlovskii, Fiz. Tekh. Poluprovodn. **35**, 769 (2001).

30. V.V. Kozlovskii, V.A. Kozlov, and V.N. Lomasov, Fiz. Tekh. Poluprovodn. **34**, 129 (2000).

31. V.I. Grafutin, A.G. Zaluzhnyi, S.P. Timoshenkov, O.M. Britkov, O.V. Ilyukhina, G.G. Myasishcheva, E.P. Prokopiev, and Yu.V. Funtikov, Zh. Èksp. Teor. Fiz. **133**, 723 (2008).

32. E.P. Prokopiev, Pis'ma Zh. Tekh. Fiz. **16**, N 24, 6 (1990).

33. S. Dannefaer, Phys. Status Solidi A **102**, 481 (1987).

34. S. Dannefaer, G.W. Dean, D.P. Kerr, and B.G. Hogg, Phys. Rev. B **14**, 2709 (1976).

35. W. Fuchs, U. Holtzhauser, S. Mantl, F.W. Richter, and F. Sturm, Phys. Status Solidi B **89**, 69 (1978).

36. S. Dannefaer, N. Fruensgaard, S. Kupca, D.P. Kerr, and B.G. Hogg, Can. J. Phys. **61**, 451 (1983).

37. S. Dannefaer, D.P. Kerr, and B.G. Hogg, J. Appl. Phys. **54**, 155 (1983).

38. J. Bourgoin and M. Lannoo, *Point Defects in Semiconductors, Vol. 2: Experimental Aspects* (Springer, Berlin, 1983).

39. E.P. Prokopiev, *Manuscript R-3634,* deposited at the Central Research Institute "Elektronika" (Moscow, 1983) (in Russian); MRS VIMI "Tekhnika, Tekhnologiya, Ekonomika" Ser. O, N 9 (1983) (in Russian).

40. H. Ikari and K. Fujiwara, J. Phys. Soc. Jpn. **46**, 92 (1979).

41. G.M. Bartenev, A.D. Tsyganov, E.P. Prokopiev, and A.Z. Varisov, Usp. Fiz. Nauk **103**, 339 (1971).

42. V.I. Grafutin, M'o Zo Khtut, E.P. Prokopiev, Yu.V. Funtikov, N.O. Khmelevskii, and Yu.V. Shtotskii, *Medical Physics* (MIFI, Moscow, 2008), Vol. 3, p. 29 (in Russian) (http://www.library.mephi.ru/data/scientific-sessions/2008/t3/0-1-9.doc).

Received 08.05.08.
Translated from Russian by O.I. Voitenko

ПОЗИТРОНІКА НАНООБ'ЄКТІВ У ПОРИСТИХ ТА ДЕФЕКТНИХ СИСТЕМАХ НА ОСНОВІ КРЕМНІЮ І КВАРЦУ

В.І. Графутін, О.В. Ілюхіна, Г.Г. М'ясищева, Е.П. Прокопьєв, С.П. Тимошенків, Ю.В. Фунтиков

Р е з ю м е

Показано, що одним із ефективних методів визначення розмірів нанооб'єктів (вакансій, вакансійних кластерів) вільних об'ємів пор, порожнин, пустот, їх концентрацій та хімічного складу в місці анігіляції в пористих системах і деяких дефектних матеріалах (і взагалі у низці технічно важливих матеріалів і наноматеріалів) є метод позитронної анігіляційної спектроскопії. Наведено короткий огляд експериментальних досліджень нанодефектів у пористому кремнії, кремнії та монокристалах кварцу, опромінених протонами, а також у порошках кварцу.